Effect of central slotted screen with a high solidity ratio on the secondary resonance phenomenon for liquid sloshing in a rectangular tank

O. M. Faltinsen,[a] R. Firoozkoohi, and A. N. Timokha
Centre for Ships and Ocean Structures and Department of Marine Technology, Norwegian University of Science and Technology, NO-7091, Trondheim, Norway

(Received 20 March 2011; accepted 3 June 2011; published online 28 June 2011)

Mounting a screen with a high solidity ratio ($0.5 \lesssim Sn < 1$) at the center of a rectangular tank qualitatively changes the secondary resonance phenomenon for liquid sloshing. In contrast to the clean tank, the steady-state sloshing due to lateral excitation is then characterized by multi-peak response curves in a neighborhood of the primary resonance frequency. The present paper revises the adaptive nonlinear multimodal method to study the secondary resonance phenomenon for the screen-affected resonant sloshing with a finite liquid depth and, thereby, clarify earlier experimental results of the authors. © *2011 American Institute of Physics*. [doi:10.1063/1.3602508]

I. INTRODUCTION

Faltinsen *et al.*[1] studied experimentally and theoretically the steady-state resonant liquid sloshing in a rectangular tank with a slat-type screen installed at the tank middle. Their application in mind was sloshing in ship tanks with swash bulkheads. It has been extensively discussed in the introduction of Ref. 1, that, in contrast to the so-called Tuned Liquid Dampers (TLDs), the swash bulkheads are characterized by a relatively large solidity ratio *Sn* (the solidity ratio is the ratio of the area of the shadow projected by the screen on a plane parallel to the screen to the total area contained within the frame of the screen). A consequence of the higher solidity ratio of a central slotted (slat-type) screen in a rectangular tank is that the *antisymmetric natural sloshing modes and frequencies* change relative to those for a clean (without screen) rectangular tank. These changes were quantified by Faltinsen and Timokha[2] versus *Sn*, the number of the screen openings (slots) *N*, and the position of these openings.

In experiments by Faltinsen *et al.*,[1] the tank was forced horizontally with the forcing frequency σ in a frequency range covering the three lowest natural sloshing frequencies of the screen-equipped tank (henceforth, σ_i^* are the natural sloshing frequencies in the clean static tank, but σ_i are the natural sloshing frequencies in the screen-equipped tank and, according to Ref. 2, $\sigma_1 < \sigma_1^* < \sigma_2 = \sigma_2^* < \sigma_3 < \sigma_3^* < \sigma_4 = \sigma_4^* < \cdots$). It was ensured that no roof impact occurred. The focus was on the liquid depth-to-tank width ratio $h/l = 0.4$ and the two forcing amplitudes $\eta_{2a}/l = 0.001$ and 0.01 (l is the tank width). Eight different screens with solidity ratios from 0.47 to 0.95 were tested. Experimental measurements of the steady-state wave elevation at the tank walls and the corresponding video observations were documented. The theoretical analysis was based on the *linear multimodal method* assuming an incompressible liquid with irrotational flow everywhere except in a local neighborhood of the screen. An "integral" viscous effect of the nearly screen flow separation on the globally inviscid liquid was governed by a pressure drop condition.[3] The latter condition yielded the $(\cdot|\cdot|)$-nonlinear damping terms in the linear modal equations and, thereby, transformed the linear modal theory to a *quasi-linear* form. When the experimental forcing amplitude was sufficiently small, $\eta_{2a}/l = 0.001$, this quasi-linear theory agreed well with the experimental response curves of the maximum steady-state wave elevations. When $\eta_{2a}/l = 0.01$, the latter modal theory gave only a general trend in how the experimental response changed versus *Sn*. Failure of the quasi-linear theory could, in part, be related to specific free-surface phenomena appearing as

(i) breaking waves,
(ii) nearly wall (screen) run-up, and
(iii) cross-flow through screen's openings from water to air with jet flow impacting on the underlying free surface.

These phenomena were illustrated by photos and videos and extensively discussed. The majority of them were established for $\sigma > \sigma_2^*$, i.e., away from the (screen-modified) lowest natural sloshing frequency $\sigma_1 < \sigma_1^*$. When σ was close to the lowest natural sloshing frequency, the aforementioned free-surface phenomena were not strong.

Another important difference between the quasi-linear predictions and experiments in Ref. 1 appears as extra peaks on the experimental response curves at which the measured steady-state wave elevations were characterized by amplification of the double harmonics, 2σ. This amplification cannot be captured by the derived quasi-linear modal theory since the only $(\cdot|\cdot|)$-nonlinear quantities of this theory yield the odd harmonics. Amplification of the double harmonics is a necessary but not sufficient condition of the *secondary resonance phenomenon* in the nonlinear free-surface sloshing problem. Faltinsen and Timokha,[4] Hermann and Timokha,[5] Ockendon *et al.*,[6] Wu,[7] and Wu and Chen[8] (see, also extended review in Chap. 8 of Ref. 9) gave theoretical and experimental analysis of the phenomenon for the two-dimensional steady-state resonant liquid sloshing in a clean rectangular tank with finite, intermediate, and shallow liquid depths. Normally, the secondary resonance is studied for the

[a]Author to whom correspondence should be addressed. Electronic mail: odd.Faltinsen@marin.ntnu.no.

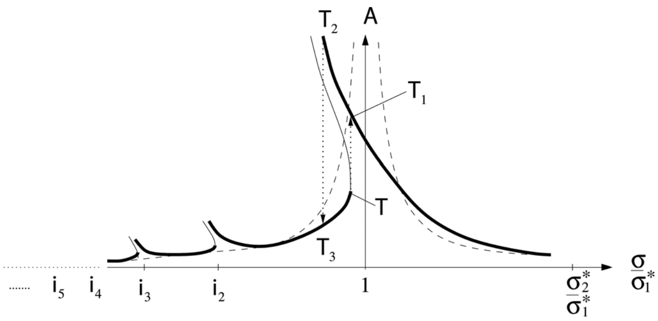

FIG. 1. The schematic response curves for a clean rectangular tank representing the maximum steady-state wave elevation A versus σ/σ_1^* for $0.3368\ldots < h/l$ due to lateral harmonic excitation. The dashed line shows results of the linear sloshing theory. The solid bold lines display stable nonlinear steady-state regimes. A hysteresis effect at $\sigma/\sigma_1^* = 1$ is possible and denoted by the points T, T_1, T_2, and T_3. The points i_2 and i_3 mark the most important secondary resonance points occurring as the forcing frequency satisfies the conditions $2\sigma = \sigma_2^*$ (amplification of the second mode) or $3\sigma = \sigma_3^*$ (amplification of the third mode), respectively. A hysteresis effect at i_2 and i_3 is also possible but, due to sufficiently large damping, it was detected in experiments[4] only for a relatively large forcing amplitude.

case when the tank is forced laterally and harmonically with the forcing frequency σ close to the lowest natural sloshing frequency σ_1^*. For the finite liquid depth (the depth-to-tank width ratio $0.2 \lesssim h/l$) and an asymptotically small forcing amplitude, the secondary resonances are mathematically expected at $2\sigma = \sigma_2^*,\ 3\sigma = \sigma_3^*, \ldots, n\sigma = \sigma_n^*, n \geq 4$. These conditions imply amplification of the second, third, and higher harmonics as well as the corresponding natural modes. The harmonics are yielded by the free-surface nonlinearities of the corresponding polynomial orders. For $0.3368\ldots < h/l$ ($0.3368\ldots$ is the so-called critical depth where the soft-to-hard spring behavior of the response curves changes with $\sigma = \sigma_1^*$), the secondary resonance peaks on the steady-state response curves are situated away from the primary resonance $\sigma = \sigma_1^*$ as shown in Fig. 1. This fact and the liquid damping cause that the peaks associated with higher-order free-surface nonlinearities (fourth, fifth, etc.) are extremely narrow and practically not realized. In contrast, the second- and third-order nonlinearities matter[4] and lead to visible peaks on the experimental response curves, especially, with increasing the forcing amplitude. The situation changes with decreasing liquid depth when the natural sloshing spectrum becomes nearly commensurate. The passage to shallow liquid depth causes finger-type response curves which are discussed and quantified by Faltinsen and Timokha[10] by employing a Boussinesq-type fourth-order multimodal method.

Based on the experimental results by Faltinsen *et al.*,[1] the aforementioned free-surface phenomena (i)–(iii) and the multi-peak response curves indicate that the nonlinearity is important for sloshing in the screen-equipped tanks, especially, with increasing the forcing amplitude. A way to describe the nonlinear liquid sloshing can be Computational Fluid Dynamics (CFD).[11] The second author attempted to model experimental cases from Ref. 1 by interFOAM, which is an OpenFOAM code that solves the two-dimensional Navier-Stokes equations for incompressible laminar two-phase flow using the volume of fluid (VOF) method for free-surface capturing and the finite volume method (FVM) for the governing equations. In these calculations, the mesh number was about 150,000. Using the Intel(R) Core(TM) 2 Quad CPU (2.5 GHz) computer with parallel computations for four sub-domains of the main domain, a computational time of about 10^5 s was required to simulate 100 s of real-time sloshing and to reach nearly steady-state conditions. This means that, even though the CFD methods are generally applicable, using them for a parameter study of the nonlinear steady-state sloshing from experiments by Faltinsen *et al.*[1] is questionable. In the present paper, we show that an alternative could be analytically oriented (e.g., asymptotic multimodal) methods based on potential flow theory and employing a pressure drop condition to capture the viscous effect associated with flow separation at the screen. The *nonlinear* adaptive multimodal method is not able to describe the phenomena (i)–(iii). However, because the higher-order nonlinearities (higher than three) do not contribute to the secondary resonance phenomenon for the finite liquid depth, the method is applicable to describe the multi-peak response curves.

The nonlinear adaptive multimodal method requires derivation of the polynomial-type modal system, i.e., the system of ordinary differential equations which keeps only up to the third-order polynomial nonlinearities in the generalized coordinates responsible for amplification of the natural sloshing modes. The adaptive modal method is a generalization of the third-order Moiseev-type theory.[12–14] The method implicitly assumes an incompressible liquid with irrotational flow, but damping due to the boundary layer at the wetted tank surface, roof impact, etc., can generally be accounted for. Considering screens with a relatively small solidity ratio, Love and Tait[15] and Love *et al.*[16] adopted the polynomial-type modal system by Faltinsen and Timokha[4] with quadratic damping terms due to viscous flow separation at the screen. Because the latter approach assumes implicitly that the natural sloshing frequencies and modes of the screen-equipped tank remain the same as those for the corresponding clean tank, it is applicable only for relatively small solidity ratios. For slotted screens, Ref. 2 estimates this fact for $0 < Sn \lesssim 0.5$. Because the natural sloshing modes are modified by the screens for $0.5 \lesssim Sn < 1$, the polynomial-type modal system by Faltinsen and Timokha[4] should be *completely revised*. Such a *revision* is reported in the present paper (see Sec. II). The newly derived modal system couples the generalized coordinates β_i responsible for the screen-modified natural modes by Faltinsen and Timokha.[2] The multimodal method assumes an incompressible liquid with irrotational flow except locally at the screen. In addition, the method requires the normal representation of the free surface and, therefore, it cannot directly account for the free-surface phenomena (i–iii) described in experiments by Faltinsen *et al.*[1,14]

To include an "integral" viscous effect due to flow separation at the screen, we employ the $(\cdot|\cdot|)$-damping terms derived in Ref. 1 from the screen-averaged pressure drop condition. These damping terms involve an integral expression of the cross-flow at the mean submerged screen part and neglect the damping caused by the free-surface phenomenon (iii). Our formulation of the pressure drop condition implicitly assumes that the cross-flow dominates relative to the tangential flow component at the screen. In addition, we neglect the fact that the tangential flow component implies a tangential drag on the screen.

Based on the results in Sec. II B, we derive in Sec. II C the required modal system keeping up to the third-order polynomial nonlinearities in terms of the generalized coordinates. Both antisymmetric and symmetric modes become coupled due to the free-surface nonlinearity. However, the screen-caused $(\cdot|\cdot|)$-damping terms appear only in modal equations responsible for the antisymmetric modes. The reason is that the antisymmetric modes determine the cross-flow, but the symmetric modes contribute to the tangential flow along the screen. In Sec. III B, the adaptive modal method by Faltinsen and Timokha[4] is generalized for the case of the screen-equipped rectangular tanks. This includes a generalization of the Moiseev asymptotic modal relationships and accounting for a larger number of the secondary resonances in a neighborhood of the lowest natural frequency. The steady-state solutions are found by combining a long-time simulations with the adaptive asymptotic modal systems and the path-following procedure along the response curves. Because the modal equations for the symmetric modes have no damping terms, we have to incorporate linear damping terms due to a viscous dissipative effect of the boundary layer flow at the mean wetted tank surface. A rough estimate of the corresponding damping rates are taken from Chap. 6 in Ref. 9. However, except for the lowest tested solidity ratio, the corresponding damping rates pass to zero in the final calculations from Sec. III.

The theoretical results in Sec. III agree well with the experimental measurements by Faltinsen *et al.*[1] for $h/l = 0.4$ and the forcing amplitude $\eta_{2a}/l = 0.01$. The theory is supported by the experimental fact that the secondary resonance peaks for $0.5 \lesssim Sn < 1$ are not only expected at i_2 and i_3 in Fig. 1, but also at

$$i_{2k} = \frac{\sigma}{\sigma_1^*} = \frac{\sigma_{2k}^*}{2\sigma_1^*} \quad (2\sigma = \sigma_{2k}^*) \quad k = 2, 3, \ldots \tag{1}$$

(due to amplification of the double harmonics) and

$$3\sigma = \sigma_{2k+1}; \quad \frac{\sigma}{\sigma_1^*} = \frac{\sigma_{2k+1}}{3\sigma_1^*} = i_{2k+1}, \quad k = 1, 2, \ldots \tag{2}$$

(due to amplification of the third harmonics).

The multimodal method has to involve twenty natural modes to describe the secondary resonance modes associated with the experiments by Faltinsen *et al.*[1] for $h/l = 0.4$ and forcing amplitude $\eta_{2a}/l = 0.01$. Moreover, many of these modes, e.g., the 13th and 15th modes, should be considered as giving the lowest-order contribution (along with the first natural mode) to handle the secondary resonance sloshing with increasing the forcing frequency to $\sigma/\sigma_1^* \approx 1.3$ and higher. The experimental observations confirmed the locally steep wave profiles. The wavelength of the 20th natural mode for the experimental 1 m tank is 10 cm, namely, the theoretically involved modes have a wavelength larger than the rough upper bound 5 cm for when surface tension matters for linear propagating capillary-gravity waves. This means that we did not make an error neglecting the surface tension in our theoretical analysis.

A possible reason for quantitative differences between our nonlinear theory and experiments in certain frequency ranges for higher solidity ratios is the use of the simplified "integral"-type pressure drop condition which neglects specific nearly screen flows. In particular, higher solidity ratios lead to a jump in the free-surface elevation at the screen which causes a cross-flow from water to air. The latter cross-flow is associated with jet flows impacting on the underlying free surface. The water-water impact is likely to represent dissipation of the total energy. At the present time, we do not have a clear strategy how to estimate contribution of this and other specific nearly screen flows on the global liquid sloshing dynamics.

II. THEORY

An incompressible liquid with irrotational two-dimensional flow is assumed everywhere in the liquid domain $Q(t)$ *except* in a small neighborhood of a screen as shown in Fig. 2. The surface tension is neglected. The two-dimensional tank has vertical walls at the free surface $\Sigma(t)$. The tank is forced horizontally with displacements $\eta_2(t)$.

A. General modal equations

We follow the general scheme of the multimodal methods described, e.g., in Chap. 7 of Ref. 9 or in Ref. 17 implying the modal solution

$$z = \zeta(y, t) = \sum_{i=1}^{\infty} \beta_i(t) f_i(y), \tag{3a}$$

$$\Phi(y, z, t) = y\,\dot{\eta}_2 + \sum_{i=1}^{\infty} R_n(t)\varphi_n(y, z) \tag{3b}$$

for the free-surface elevation and the absolute velocity potential, respectively. Here, β_i and R_n are the generalized coordinates and $\varphi_n(f_n(y) = \varphi_n(y, 0))$ are the natural sloshing modes which are the eigenfunctions of the boundary spectral problem,

$$\nabla^2\varphi_n = 0 \text{ in } Q_0; \; \frac{\partial\varphi_n}{\partial n} = 0 \text{ on } S_0;$$
$$\frac{\partial\varphi_n}{\partial z} = \kappa_n\varphi_n \text{ on } \Sigma_0; \; \int_{\Sigma_0} \varphi_n \mathrm{d}y = 0, \tag{4}$$

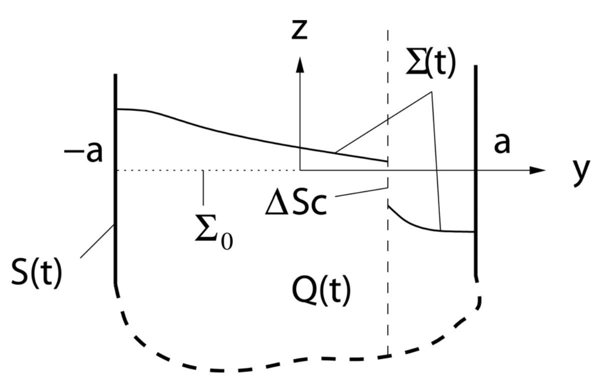

FIG. 2. A general two-dimensional tank with vertical walls near the free surface and, possibly, a perforated vertical screen. In our modal theory, the liquid cross-flow at the screen part ΔSc with subsequent fallout of the screen-generated liquid jet impact on the free surface is neglected; this cannot be described by the modal solution (3a).

where Q_0 is the mean liquid domain, S_0 is the mean wetted tank surface including the solid screen parts, and Σ_0 is the mean free surface. The natural sloshing frequencies are computed by the formulas $\sigma_n = \sqrt{g\kappa_n}$, $n = 1, 2, \ldots$ (g is the gravity acceleration).

The multimodal method employs the modal solution (3) with the normal presentation of the free surface (3a) and, thereby, *implicitly assumes* that there are no overturning waves. Since any breaking waves involve vorticity generation, they also cannot be described. Moreover, as it is shown in Fig. 2, the modal solution (3a) *cannot* model the liquid flow through the screen part ΔSc where one side of the screen is wetted, but another dry contacting the ullage gas. Experimental observations by Faltinsen *et al.*[1] reported a flow through ΔSc with forthcoming water fallout on the free surface. The multimodal method neglects this flow.

Chapter 7 in Ref. 9 shows that using the modal solution (3) together with the Bateman-Luke variational principle leads to the following general [modal] infinite-dimensional system of ordinary differential equations,

$$\sum_{k=1}^{\infty} \frac{\partial A_n}{\partial \beta_k}\dot{\beta}_k = \sum_{k=1}^{\infty} A_{nk}R_k, \quad n = 1, 2, \ldots, \tag{5a}$$

$$\sum_{n=1}^{\infty} \frac{\partial A_n}{\partial \beta_\mu}\dot{R}_n + \frac{1}{2}\sum_{n,k=1}^{\infty} \frac{\partial A_{nk}}{\partial \beta_\mu}R_nR_k + g\Lambda_{\mu\mu}^{(0)} + \lambda_{2\mu}\ddot{\eta}_2 = 0, \quad \mu = 1, 2, \ldots \tag{5b}$$

which couple the generalized coordinates β_k and R_n introduced by the modal solution (3). Here,

$$A_n = \int_{Q(t)} \varphi_n \mathrm{d}Q; \quad A_{nk} = \int_{Q(t)} \nabla\varphi_n \cdot \nabla\varphi_k \mathrm{d}Q;$$
$$\lambda_{2n} = \int_{\Sigma_0} y f_n \mathrm{d}S; \quad \Lambda_{nn}^{(0)} = \int_{\Sigma_0} f_n^2 \mathrm{d}S \tag{6}$$

so that A_n and A_{nk} are nonlinear functions of β_i.

Generally speaking, the fully nonlinear modal system (5) can be adopted for direct simulations. Going this way means the so-called Perko's[18,19] method. La Rocca *et al.*[20] used this method to describe nonlinear liquid sloshing in a clean rectangular tank. Simulations by the Perko method are less numerically efficient than the use of the adaptive modal method. However, the main problem of the Perko-type methods is that the system (5) becomes numerically stiff for strongly resonant sloshing. The latter fact has been discussed by Faltinsen and Timokha.[4,10]

B. The polynomial-type modal equations

In accordance with the adaptive multimodal method by Faltinsen and Timokha,[4] we assume that the nonlinear intermodal interaction is primarily determined by the second- and third-order polynomial terms in the generalized coordinates. This means that one can reduce (5) by keeping the third-order polynomial quantities. Using the Taylor series at $z = 0$

$$\varphi(y, \zeta, t) = f_n + (\kappa_n f_n)\zeta + \frac{1}{2}\left(\sum_{l=1}^{\infty} \alpha_{n,l} f_l\right)\zeta^2 + \cdots$$

in the expression

$$\frac{\partial A_n}{\partial \beta_k} = \int_{-a}^{a} \varphi(y, \zeta, t) f_k \,\mathrm{d}y$$

as well as in the expression on p. 173 of Ref. 4, i.e.,

$$A_{nk} = \kappa_n\Lambda_{nk}^{(0)} + \int_{-a}^{a} (\nabla\varphi_n \cdot \nabla\varphi_k)|_{z=0}\,\zeta\,\mathrm{d}y + \frac{1}{2}\int_{-a}^{a} \left.\frac{\partial(\nabla\varphi_n \cdot \nabla\varphi_k)}{\partial z}\right|_{z=0} \zeta^2\,\mathrm{d}y + \cdots$$

gives the formulas

$$\frac{\partial A_n}{\partial \beta_j} = \Lambda_{nj}^{(0)} + \kappa_n\sum_{i=1}^{\infty}\Lambda_{nji}^{(1)}\beta_i + \frac{1}{2}\sum_{i,k=1}^{\infty}\left(\sum_{m=1}^{\infty}\alpha_{n,m}\Lambda_{mjik}^{(2)}\right)\beta_i\beta_k + \cdots, \tag{7}$$

$$A_{nk} = \kappa_n\Lambda_{nk}^{(0)} + \sum_{i=1}^{\infty}\Pi_{nk,i}^{(1)}\beta_i + \frac{1}{2}\sum_{p,q=1}^{\infty}\Pi_{nk,pq}^{(2)}\beta_p\beta_q + \cdots. \tag{8}$$

Here, we used the following relations:

$$f_n(y) = \varphi_n(y, 0); \quad \kappa_n f_n = \left.\frac{\partial\varphi_n}{\partial z}\right|_0; \quad \sum_{l=1}^{\infty}\alpha_{n,l}f_l = \left.\frac{\partial^2\varphi_n}{\partial z^2}\right|_0, \tag{9a}$$

$$\frac{\partial f_n}{\partial y} = \left.\frac{\partial\varphi_n}{\partial y}\right|_0; \quad \kappa_n\frac{\partial f_n}{\partial y} = \left.\frac{\partial^2\varphi_n}{\partial y\partial z}\right|_0; \quad \sum_{l=1}^{\infty}\alpha_{n,l}\frac{\partial f_l}{\partial y} = \left.\frac{\partial^3\varphi_n}{\partial y\partial z^2}\right|_0, \tag{9b}$$

where the coefficients $\alpha_{n,l}$ are introduced which imply a Fourier expansion of $\partial^2\varphi_n/\partial z^2|_{z=0}$ in terms of the orthogonal basis $\{f_n\}$;

$$\int_{-a}^{a} f_n f_k\,\mathrm{d}y = \Lambda_{nk}^{(0)}; \quad \int_{-a}^{a} f_n f_k f_i\,\mathrm{d}y = \Lambda_{nki}^{(1)};$$
$$\int_{-a}^{a} f_n f_k f_i f_j\,\mathrm{d}y = \Lambda_{nkij}^{(2)} \ldots, \tag{10}$$

$$\int_{-a}^{a}\frac{\partial f_n}{\partial y}\frac{\partial f_k}{\partial y}f_i\,\mathrm{d}y = \Lambda_{nk,i}^{(-1)}; \quad \int_{-a}^{a}\frac{\partial f_n}{\partial y}\frac{\partial f_k}{\partial y}f_i f_j\,\mathrm{d}y = \Lambda_{nk,ij}^{(-2)}, \ \ldots, \tag{11}$$

where, due to the orthogonality of the natural modes, $\Lambda_{nk}^{(0)} = 0$, $n \neq k$,

$$\Pi_{nk,i}^{(1)} = \Lambda_{nk,i}^{(-1)} + \kappa_n\kappa_k\Lambda_{nki}^{(1)}, \tag{12a}$$

$$\Pi_{nk,pq}^{(2)} = (\kappa_n + \kappa_k)\Lambda_{nk,pq}^{(-2)} + \sum_{m=1}^{\infty}\left[\alpha_{n,m}\kappa_k\Lambda_{mkpq}^{(2)} + \alpha_{k,m}\kappa_n\Lambda_{mnpq}^{(2)}\right]. \tag{12b}$$

The comma is used between indexes which disallow their position exchange. As long as there is no comma between the indexes, these indexes can commutate.

Substituting

$$R_k = \frac{\dot{\beta}_k}{\kappa_k} + \sum_{p,q=1}^{\infty}V_{p,q}^{2,k}\dot{\beta}_p\beta_q + \sum_{p,q,m=1}^{\infty}V_{p,q,m}^{3,k}\dot{\beta}_p\beta_q\beta_m + \cdots \tag{13}$$

in the kinematic equation (5a), one can compute the coefficients,

$$V_{k,i}^{2,n} = \frac{1}{\kappa_n \Lambda_{nn}^{(0)}} \left[-\frac{\Pi_{nk,i}^{(1)}}{\kappa_k} + \kappa_n \Lambda_{nki}^{(1)} \right], \tag{14a}$$

$$V_{k,p,q}^{3,n} = \frac{1}{\kappa_n \Lambda_{nn}^{(0)}} \left[-\frac{\Pi_{nk,pq}^{(2)}}{2\kappa_k} + \sum_{m=1}^{\infty} \left(\tfrac{1}{2}\alpha_{n,m} \Lambda_{mkpq}^{(2)} - \Pi_{nm,p}^{(1)} V_{k,q}^{2,m} \right) \right] \dots \tag{14b}$$

Finally, using Eqs. (7), (8), and (13) in the dynamic modal equation (5b), one can find the following asymptotic modal equation accounting for the third-order components in terms of the generalized coordinates β_i,

$$\sum_{n=1}^{\infty} \ddot{\beta}_n \left[\delta_{n\mu} + \sum_{i=1}^{\infty} d_{n,i}^{1,\mu} \beta_i + \sum_{i,j=1}^{\infty} d_{n,i,j}^{2,\mu} \beta_i \beta_j \right] + \\ + \sum_{n,k=1}^{\infty} \dot{\beta}_n \dot{\beta}_k \left[t_{n,k}^{0,\mu} + \sum_{i=1}^{\infty} t_{n,k,i}^{1,\mu} \beta_i \right] + \sigma_\mu^2 \beta_\mu + P_\mu \ddot{\eta}_2 = 0, \\ \mu = 1, 2, \dots, \tag{15}$$

where

$$\sigma_\mu^2 = g\kappa_\mu; \quad P_\mu = \frac{\kappa_\mu \lambda_{2\mu}}{\Lambda_{\mu\mu}^{(0)}}, \tag{16a}$$

$$d_{n,i}^{1,\mu} = \kappa_\mu \left(V_{n,i}^{2,\mu} + \frac{\Lambda_{n\mu i}^{(1)}}{\Lambda_{\mu\mu}^{(0)}} \right); \quad t_{n,k}^{0,\mu} = \kappa_\mu V_{n,k}^{2,\mu} + \frac{\kappa_\mu \Pi_{nk,\mu}^{(1)}}{2\kappa_n \kappa_k \Lambda_{\mu\mu}^{(0)}}, \tag{16b}$$

$$d_{n,i,j}^{2,\mu} = \kappa_\mu \left(V_{n,j,i}^{3,\mu} + \frac{1}{\Lambda_{\mu\mu}^{(0)}} \sum_{m=1}^{\infty} \left[\kappa_m \Lambda_{m\mu i}^{(1)} V_{n,j}^{2,m} + \frac{1}{2} \frac{\alpha_{n,m} \Lambda_{m\mu ij}^{(2)}}{\kappa_n} \right] \right), \tag{16c}$$

$$t_{n,k,i}^{1,\mu} = \kappa_\mu \Bigg(V_{n,k,i}^{3,\mu} + V_{n,i,k}^{3,\mu} + \frac{\Pi_{nk,\mu i}^{(2)}}{2\kappa_n \kappa_k \Lambda_{\mu\mu}^{(0)}} + \frac{1}{2\Lambda_{\mu\mu}^{(0)}} \sum_{m=1}^{\infty} \\ \times \left[2\kappa_m \Lambda_{m\mu i}^{(1)} V_{n,k}^{2,m} + \frac{\Pi_{mk,\mu}^{(1)} V_{n,i}^{2,m}}{\kappa_k} + \frac{\Pi_{nm,\mu}^{(1)} V_{k,i}^{2,m}}{\kappa_n} \right] \Bigg). \tag{16d}$$

C. Modal equations for the case of a central slotted screen

The two-dimensional liquid sloshing is considered in a rectangular tank with width $l = 2a$ and a slotted screen installed at the tank middle as shown in Fig. 3. The figure introduces the geometric notations and the body-fixed coordinate system. The screen appears as a thin solid plate with a series of perforated horizontal slots. The screen thickness is neglected. When the liquid is at rest, the wetted screen part Sc_0 has N submerged slots. The *solidity ratio* of the submerged screen part is denoted by Sn which is a function of h and N.

Under assumptions of the previous section, we use the modal equations (15) in which the hydrodynamic coefficients

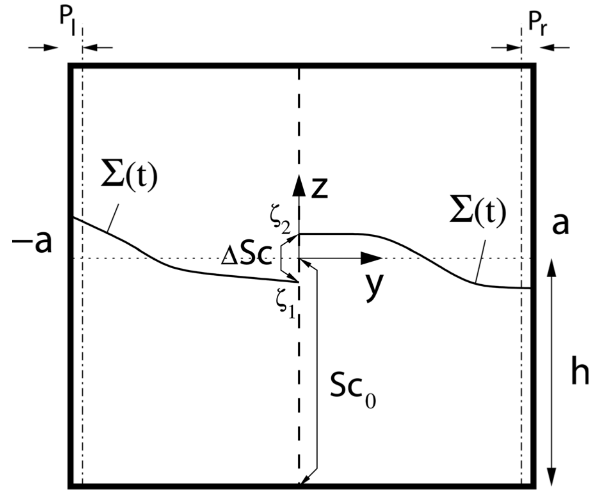

FIG. 3. A schematic picture of a rectangular tank with a slat-type screen in the middle. Basic geometric notations. Two measurement probes of wave elevation are located at small distances P_l and P_r from the walls. The mean wetted screen is Sc_0. For higher solidity ratios, the free surface $\Sigma(t)$ has a clear jump at the screen formed by the "wet-dry" area ΔSc (here, the interval (ζ_1,ζ_2)).

are computed based on the natural sloshing modes by Faltinsen and Timokha.[2] For $0.5 \lesssim Sn < 1$, these hydrodynamic coefficients are functions of Sn and N as well as slot positions. The modal equations do not account for a local viscous flow through the screen. Following Faltinsen *et al.*,[1] this can be done by employing an "integral" (averaged) version of the pressure drop condition[3] defined on the mean wetted screen as follows:

$$P_- - P_+ = \frac{1}{2}\rho K u|u| \quad \text{on} \quad Sc_0, \tag{17}$$

where K is an empirical pressure drop coefficient, ρ is the liquid density, u is the so-called lateral *approach* velocity to the screen, and $(P_- - P_+)$ is the *pressure drop*. A review on using this condition in sloshing problems can be found in Refs. 1, 9, and 21. This empirical condition comes from the steady-flow case[3] and, generally, can be employed for sloshing problems with many screens installed at different places. The space-averaged version of the pressure drop formulation (17) assumes that both sides of the screen are wetted, i.e. the jump $|\Delta Sc| = \zeta_2 - \zeta_1$ in Fig. 3 and the liquid flow through ΔSc are neglected. The pressure drop coefficient K depends on the solidity ratio Sn. It may also depend on the Reynolds and Keulegan-Carpenter (KC) numbers. For slat-type screens, the pressure drop coefficient weakly depends on the Reynolds number. There is negligible dependence on KC number for relevant KC numbers. Following Tait *et al.*[21] and Faltinsen *et al.*,[1] we will adopt the following approximation of the empirical pressure drop coefficient:

$$K = \left(\frac{1}{Cc\,(1 - Sn)} - 1 \right)^2, \quad Cc = 0405 \exp(-\pi Sn) + 0.595 \\ \text{for} \quad Sn \geq 03. \tag{18}$$

The formula (18) is applicable for different Sn-values. According to experimental values of K by Blevins,[3] its relative accuracy is less than 20% for $Sn \leq 0.9$, but may be larger for $Sn \geq 0.9$.

Faltinsen *et al.*[1] showed that the "integral" pressure drop condition leads to the following quantities:

$$KD_m(\dot\beta_{2i-1}) = -K\frac{\alpha'_m\kappa_{2m-1}}{4h\Lambda^{(0)}_{(2m-1)(2m-1)}}\int_{-h}^{0}\left(\sum_{i=1}^{\infty}\frac{\dot\beta_{2i-1}}{\kappa_{2i-1}}U_i(z)\right)\times\left|\sum_{i=1}^{\infty}\frac{\dot\beta_{2i-1}}{\kappa_{2i-1}}U_i(z)\right|\mathrm{d}z \qquad (19)$$

to be incorporated into the modal equations for the antisymmetric modes (generalized coordinates β_{2m-1}) responsible for cross-flow through the screen. Here

$$\alpha'_m = 2\int_{-a}^{0} f_{2m-1}\mathrm{d}y,$$
$$U_i(z) = -\frac{1}{a}\cosh(k_0^{(i)}(z+h)/a)\sin(k_0^{(i)}),$$

with the constant $k_0^{(i)}$ being the roots of the equations,

$$k_0^{(i)}\tanh(k_0^{(i)}h/a) = \kappa_{2i-1}a.$$

Using the modal equations (15) and the pressure-drop "integral" terms (19) leads to the following modal equations:

$$\sum_{n=1}^{\infty}\ddot\beta_n\left[\delta_{n(2m-1)}+\sum_{i=1}^{\infty}D1^{2m-1}(n,i)\beta_i + \sum_{j=1}^{\infty}\sum_{i=1}^{j}D2^{2m-1}(n,i,j)\beta_i\beta_j\right] + \sum_{n=1}^{\infty}\sum_{k=1}^{n}\dot\beta_n\dot\beta_k\left[T0^{2m-1}(n,k)+\sum_{i=1}^{\infty}T1^{2m-1}(n,k,i)\beta_i\right] + KD_m(\dot\beta_{2i-1}) + \sigma^2_{2m-1}\beta_{2m-1} + P_{2m-1}\ddot\eta_2 = 0, \qquad (20a)$$

$$\sum_{n=1}^{\infty}\ddot\beta_n\left[\delta_{n(2m)}+\sum_{i=1}^{\infty}D1^{2m}(n,i)\beta_i + \sum_{j=1}^{\infty}\sum_{i=1}^{j}D2^{2m}(n,i,j)\beta_i\beta_j\right] + \sum_{n=1}^{\infty}\sum_{k=1}^{n}\dot\beta_n\dot\beta_k\left[T0^{2m}(n,k)+\sum_{i=1}^{\infty}T1^{2m}(n,k,i)\beta_i\right] + \sigma^2_{2m}\beta_{2m} = 0, \quad m=1,2,\ldots, \qquad (20b)$$

where

$$D1^{\mu}(n,i) = d^{1,\mu}_{n,i};\qquad D2^{\mu}(n,i,j) = \begin{cases} d^{2,\mu}_{n,i,i}, & i=j,\\ d^{2,\mu}_{n,i,j}+d^{2,\mu}_{n,j,i}, & i\neq j,\end{cases}$$
$$T0^{\mu}(n,k) = \begin{cases} t^{0,\mu}_{n,n}, & n=k,\\ t^{0,\mu}_{n,k}+t^{0,\mu}_{k,n}, & n\neq k,\end{cases}$$
$$T1^{\mu}(n,k,i) = \begin{cases} t^{1,\mu}_{n,n,i}, & n=k,\\ t^{1,\mu}_{n,k,i}+t^{1,\mu}_{k,n,i}, & n\neq k.\end{cases}$$

As we remarked above, the hydrodynamic coefficients in the modal equations (20) are computed by using the natural sloshing modes from Ref. 2.

When $0 < Sn \lesssim 0.5$, the natural sloshing modes are close to those for the clean tank, i.e., these are approximately governed by the trigonometric algebra implying

$$\varphi_k(y,z) \approx \cos\left(\frac{\pi k}{a}(y-a)\right)\frac{\cosh(\pi k(z+h)/l)}{\cosh(\pi kh/l)}, \qquad (21)$$

in expressions of Sec. II B. As a consequence, many of the hydrodynamic coefficients at the polynomial-type terms of (20) are zero. In particular, the quadratic nonlinearity in β_1 (the generalized coordinate responsible for the first mode) is only present in the first equation of (20b) governing the first symmetric mode (β_2). Analogously, the cubic terms in β_1 exist only in the first and second equations of (20a). This means that the secondary resonance due to the second harmonics can only excite the second mode, but the third harmonics can only lead to the secondary resonance for the third mode.

When $0.5 \lesssim Sn < 1$, the trigonometric algebra representation for the natural sloshing modes (21) breaks down so that the screen-effected antisymmetric modes become, generally, non-continuous in the center of Σ_0 (see examples in Ref. 2). This fact leads to additional nonzero hydrodynamic coefficients causing a complex nonlinear energy redistribution between lower and higher modes. So, the nonzero quadratic quantities in β_1 appear now in all the equations for even modes (20b), i.e., all the symmetric modes can be amplified due to the second harmonics (the second-order nonlinearity) but the nonzero cubic terms in β_1 are present in all the equations (20a). As a consequence, the higher solidity ratios yield the secondary resonance due to the second and third harmonics not only at i_2 and i_3 but also at i_k, $k \geq 2$ defined by Eqs. (1) and (2).

Incorporating the $KD_m(\dot\beta_{2i-1})$-terms in modal equations (20a) adds a quadratic damping into a conservative mechanical system with infinite degrees of freedom. Because we operate with potential flow theory, the modal equations (20) do not contain other damping terms, e.g., due to laminar viscous boundary layer, tangential viscous drag at the screen, and wave breaking. Moreover, because the symmetric modes do not cause cross-flow through the central screen, the modal equations (20b) do not have any damping terms at all. As it will be explained in detail in Sec. III C, the latter fact can make it difficult to find the steady-state solution due to a continuous beating by these symmetric modes. Artificial small damping is therefore needed to reach the steady-state condition. For this purpose, it is standard procedure to incorporate the linear damping terms,

$$2\alpha_i\sigma_i\dot\beta_i \qquad (22)$$

in the ith equation of (20) to account for other damping mechanisms and prevent the aforementioned beating in the computations. The actual values of α_i are unknown and, according to our theoretical model, should pass to zero in final calculations after the steady-state condition is achieved. A rough estimate of the initial α_i-values adopted for our steady-state calculations can be associated with the damping rates ξ_i for *linear sloshing* due to the laminar viscous boundary layer at the mean wetted tank surface for the clean tank evaluated in Secs. 6.3.1 and 6.11.1 of Ref. 9. The corresponding numerical procedure on the steady-state solution with decreasing α_i is explained in Sec. III C.

III. RESONANT STEADY-STATE SLOSHING DUE TO LATERAL EXCITATION WITH THE FORCING FREQUENCY AT THE LOWEST NATURAL SLOSHING FREQUENCY

A. Nondimensional formulation

We assume that $\eta_2(t) = \eta_{2a}\cos(\sigma t)$ with a relatively small nondimensional forcing amplitude η_{2a}/l and σ being close to the lowest natural sloshing frequency σ_1^* of the corresponding clean tank. The liquid depth is finite. Henceforth, we will introduce asymptotic relationship between the l-scaled generalized coordinates. This needs rewriting the modal equations (20) in a nondimensional form. Introducing the characteristic length $l = 2a$ and the characteristic time $t_* = 1/\sigma_1^*$, the normalization transforms the modal equations to the form,

$$\begin{aligned}
&\sum_{n=1}^{\infty}\ddot{\bar\beta}_n\left[\delta_{n(2m-1)} + \sum_{i=1}^{\infty}\bar D1^{2m-1}(n,i)\bar\beta_i\right.\\
&\quad\left. + \sum_{j=1}^{\infty}\sum_{i=1}^{j}\bar D2^{2m-1}(n,i,j)\bar\beta_i\bar\beta_j\right] + \sum_{n=1}^{\infty}\sum_{k=1}^{n}\dot{\bar\beta}_n\dot{\bar\beta}_k\\
&\quad\times\left[\bar T0^{2m-1}(n,k) + \sum_{i=1}^{\infty}\bar T1^{2m-1}(n,k,i)\bar\beta_i\right]\\
&\quad + 2\alpha_{2m-1}\bar\sigma_{2m-1}\dot{\bar\beta}_{2m-1} + K\bar D_m(\dot{\bar\beta}_{2i-1})\\
&\quad + \bar\sigma_{2m-1}^2\bar\beta_{2m-1} - \bar\eta_{2a}\bar\sigma\cos(\bar\sigma t) = 0,
\end{aligned} \tag{23a}$$

$$\begin{aligned}
&\sum_{n=1}^{\infty}\ddot{\bar\beta}_n\left[\delta_{n(2m)} + \sum_{i=1}^{\infty}\bar D1^{2m}(n,i)\bar\beta_i + \sum_{j=1}^{\infty}\sum_{i=1}^{j}\bar D2^{2m}(n,i,j)\bar\beta_i\bar\beta_j\right]\\
&\quad + \sum_{n=1}^{\infty}\sum_{k=1}^{n}\dot{\bar\beta}_n\dot{\bar\beta}_k\left[\bar T0^{2m}(n,k) + \sum_{i=1}^{\infty}\bar T1^{2m}(n,k,i)\bar\beta_i\right]\\
&\quad + 2\alpha_{2m}\bar\sigma_{2m}\dot{\bar\beta}_{2m} + \bar\sigma_{2m}^2\bar\beta_{2m} = 0, \quad m = 1,2,\ldots.
\end{aligned} \tag{23b}$$

Here, we have incorporated the linear damping terms (22) and introduced the following nondimensional variables:

$$\begin{aligned}
&\bar\beta_i = \beta_i/l,\quad \bar\eta_{2a} = \eta_{2a}/l,\quad \bar\sigma = \sigma/\sigma_1^*,\quad \bar\sigma_i = \sigma_i/\sigma_1^*,\\
&\bar D1^i = l D1^i,\quad \bar D2^i = l^2 D2^i,\quad \bar T0^i = l\,T0^i,\quad \bar T1^i = l^2\,T1^i,\\
&\bar D_m(\dot{\bar\beta}_i) = l\,D_m(l\dot{\bar\beta}_i)
\end{aligned}$$

B. Generalization of the adaptive asymptotic modal method

Working with the clean rectangular tank, Faltinsen and Timokha[4] proposed an adaptive asymptotic modal method for the resonant steady-state liquid sloshing. They assumed that the forcing amplitude is small, $\bar\eta_{2a} = O(\epsilon)$, $\epsilon \ll 1$ and that σ is in a neighborhood of σ_1^*. The method starts with the Moiseev[12–14] third-order asymptotic relationships,

$$\bar\beta_1 = O(\epsilon^{1/3}), \bar\beta_2 = O(\epsilon^{2/3}), \bar\beta_3 = O(\epsilon), \bar\beta_k \lesssim O(\epsilon), k \ge 4, \tag{24}$$

considering them as *a priori* estimate of the generalized coordinates $\bar\beta_i$.

Based on the asymptotic relationships (24), one can derive the corresponding asymptotic modal equations by neglecting the $o(\epsilon)$-terms in the polynomial-type modal equations (23). This was done by Faltinsen *et al.*[14] Further, Faltinsen *et al.*[14] and Faltinsen and Timokha[4] showed that the asymptotic relations (24) are not satisfied when σ/σ_1^* in close to i_2 and i_3 (see Fig. 1) on the asymptotic scale $O(\epsilon^{2/3})$. The use of the asymptotic modal equations by Faltinsen *et al.*[14] leads then to unrealistic amplification of the generalized coordinates $\bar\beta_2$ and $\bar\beta_3$. When this happened, Faltinsen and Timokha[4] proposed *a posteriori* asymptotic relationships considering $\bar\beta_2$ and/or $\bar\beta_3$ to have the dominant order $O(\epsilon^{1/3})$. Neglecting the $o(\epsilon)$-terms in (23) makes it possible to derive the corresponding asymptotic modal equations based on these new asymptotic relationships. References 4 and 22 demonstrate that the same forcing amplitude and frequency can require different asymptotic modal systems (asymptotic ordering) for steady-state solutions belonging to different response curves.

According to the Moiseev asymptotics (24) for the clean tank, there is only one dominant mode $(\bar\beta_1)$ and only one mode $(\bar\beta_2)$ possesses the second asymptotic order. However, as we have already commented, the non-zero second-order polynomial terms in $\bar\beta_1$ appear for $0.5 \lesssim Sn < 1$ in all the modal equations (23b) but the nonzero cubic terms in $\bar\beta_1$ are now presented in (23a). This means that the Moiseev-type asymptotics (24) should in the studied case change to

$$\bar\beta_1 = O(\epsilon^{1/3}),\quad \bar\beta_{2k} = O(\epsilon^{2/3}),\quad \bar\beta_{2k+1} = O(\epsilon),\quad k \ge 2 \tag{25}$$

and, in contrast to the clean tank with a finite liquid depth considering only two possible secondary resonances for $\bar\sigma$ close to the points i_2 and i_3, we should now expect the multiple secondary resonances as $\bar\sigma$ is close to values from the sets (1) and (2). Thus, we see that screens with $0.5 \lesssim Sn < 1$ change the Moiseev asymptotics (24) to (25) and, besides, the secondary resonances should now be expected at i_k, $k \ge 2$. These facts modify the adaptive modal method.

We start now with (25) as *a priori* asymptotics. When considering a frequency range $\bar\sigma_a < \bar\sigma < \bar\sigma_b$, we should further find out whether there are any i_k belonging (being close) to this range and change the ordering of the generalized coordinates $\bar\beta_k$ in Eq. (25) to $\bar\beta_k = O(\epsilon^{1/3})$ for the corresponding indexes k. This will be *a posteriori* asymptotics. To obtain the corresponding asymptotic modal system, we should exclude the $o(\epsilon)$-terms in modal equations (23). By using direct simulations with these *a posteriori* asymptotic modal equations, one must also validate whether we have included all the dominant generalized coordinates on the studied interval $\bar\sigma_a < \bar\sigma < \bar\sigma_b$. If not, more dominant modes should be added.

We must note that we have an extra term $K\bar D_m$ in Eqs. (23a) where, because $\bar D_m$ is of the quadratic character with respect to $\bar\beta_1$, $\bar D_m = O(\epsilon^{2/3})$. The asymptotic modal equations include the asymptotic quantities up to the order $O(\epsilon)$ and, therefore, our asymptotic scheme requires $\epsilon^{1/3} \lesssim K$. When the $K\bar D_m$-terms are of either comparable or lower order with respect to the dominant $\epsilon^{1/3}$, these terms give a leading contribution to the nonlinear resonant sloshing. This condition implies

$$O(\epsilon^{-1/3}) = \bar{\eta}_{2a}^{-1/3} \lesssim K. \qquad (26)$$

C. Numerical steady-state solution

Normally, the numerical steady-state solution of the nonlinear adaptive asymptotic modal system is found by a long-time simulation with appropriate damping terms (see Refs. 1, 4, and 22). For the clean tank,[4] the linear damping coefficients (22) are used to get a numerical steady-state solution by means of these simulations. Nevertheless, the first approximation is found with $\alpha_i \geq \xi_i$ but next approximations follow from the long-time simulations with lower values of α_i and initial conditions following from the previous steady-state solution computed with a larger α_i. Faltinsen and Timokha[4] report that such a numerical procedure with a stepwise decrease of the damping ratios practically converges with $\alpha_i \lesssim \xi_i/100$ so that the corresponding numerical steady-state solution obtained with $\alpha_i \approx \xi_i/100$ can be considered as the steady-state solution of the corresponding asymptotic modal system without damping terms. Moreover, the experimentally established secondary-resonance jumps between the steady-state solutions for the clean tank (as in Fig. 1) were detected for $\alpha_i \lesssim \xi/100$. This means that, due to possible nonlinear character of damping, the adopted linear damping rates for nonlinear steady-state motions can be lower than ξ_i, but theserates should be higher for the resonance-type transients.

In the studied case, the subsystem for antisymmetric modes has, by definition, the unavoidable quadratic damping terms. However, the subsystem (20b) describing the symmetric modes has not any proper damping terms. This "disproportion" between symmetric and antisymmetric modes can affect the time-step simulations leading to a long-time non-decaying beating by the symmetric modes. As a consequence, whereas we can in the majority of cases postulate $\alpha_{2m-1} = 0$ in Eq. (23a), the damping ratios α_{2m} in Eq. (23b) should not be zero in simulations to describe the steady-state sloshing.

In the next section, we will typically take $\alpha_{2m-1} = 0$, $\alpha_{2m} = \xi_{2m}$ to get the first approximation of the steady-state solution. The next approximations will be obtained by long-time simulations with initial conditions following from the previous steady-state solution and lower values of α_{2m}. Except for the case of lower Sn with K that, generally, does not satisfy (26), this recursive procedure in α_{2m} for getting the numerical steady-state solution will practically converge with $\alpha_{2m} \lesssim \xi_{2m}/10$. Similar to numerical results by Faltinsen and Timokha[4] for the clean tank, the secondary-resonance jumps become detected after the procedure converges with a lower tested α_{2m}. The subsequent decrease of α_{2m} does not influence the result (difference is less that 0.1%), but may in some cases cause numerical instability on the long-time scale due to the stiffness of the ordinary differential equations. The Adams-Bashforth-Moulton predictor-corrector algorithm of orders 1 through 12 is involved in our computations. The algorithm handles mildly stiff differential equations.

The numerical recursive procedure in α_{2m} is combined with a path-following procedure along the response branches by a stepwise change of $\bar{\sigma}$ in positive and negative directions. This path-following procedure makes it possible to go along the steady-state response curves and, thereby, detect jumps between branches. However, it does not guarantee that no more branches exist.

D. Theoretical and experimental secondary-resonance response curves

Using the adaptive multimodal method we will study the secondary resonance phenomenon in a screen-equipped rectangular tank by considering the experimental case from Ref. 1 for $\bar{\eta}_{2a} = \eta_{2a}/l = 0.01$, $\bar{h} = h/l = 0.4$, and seven different screens. The screens' structure and experimental setup are in some detail described in Ref. 1. Even though Faltinsen *et al.*[1] tested the frequency range $0.7 < \sigma/\sigma_1^* < 2.2$, our primary focus will be on the interval $0.7 < \sigma/\sigma_1^* < 1.36$. The upper bond of the interval is chosen to be away from $1.52 = \sigma_2/\sigma_1^* < \sigma_3/\sigma_1^*$. The reason is that the experimental steady-state sloshing with $\sigma_2^*/\sigma_1^* \lesssim \bar{\sigma}$ (the forcing frequency exceeds the second natural sloshing frequency) is characterized by the free-surface phenomena mentioned in Introduction as (i-iii). The multimodal method is not able to describe them.

Within the framework of the experimental input parameters, the calculation by the adaptive modal method established stabilization of the numerical steady-state solution (error is less than 0.01%) by twenty generalized coordinates (describing amplification of ten symmetric and ten antisymmetric modes). Further, to cover the frequency range $0.7 < \sigma/\sigma_1^* < 1.36$, we needed four different adaptive modal systems (asymptotic orderings) whose domains of applicability are overlapped and shown in Figs. 4, 6, 8, 9, and 11.

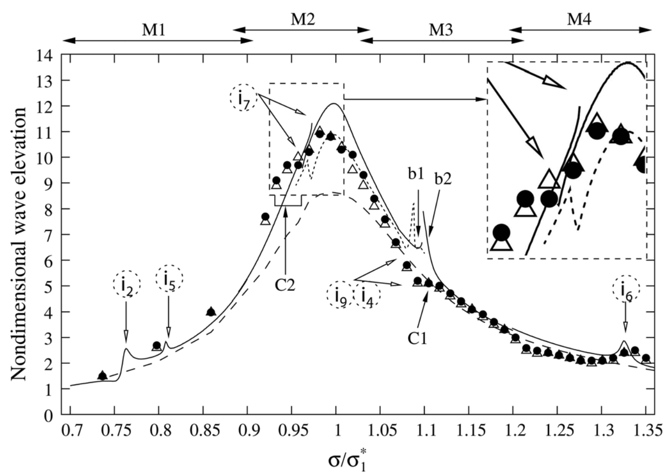

FIG. 4. The theoretical and experimental η_{2a}-scaled maximum wave elevation at the walls; $h/l = 0.4$ and $\eta_{2a}/l = 0.01$. The signs (•) and (Δ) denote the experimental measurements done at opposite walls (1 cm away from the walls, respectively). The submerged screen part has at rest 70 opening (slots), $Sn = 0.4725$ with $K = 3.09862$ (according to (18)). The solid lines denote results by the adaptive modal method involving four different asymptotic modal systems M1, M2, M3, and M4, whose frequency ranges are shown on the top. The modal systems involve $\alpha_{2m} = \xi_{2m}$ in Eq. (23b) and $\alpha_{2m-1} = 0$ in Eq. (23a). The dotted line in the middle shows the results with $\alpha_m = \xi_m$ in Eq. (23). The dashed line (quasi-linear modal theory) is taken from Faltinsen *et al.*[1] The values i_k are defined by Eqs. (1) and (2). They imply possibility of secondary resonance due to amplification of the second and third harmonics. The response curves are not connected between the branches b1 and b2 (a combined i_9-and-i_4 resonance) and in the zoomed zone caused by the secondary resonance at i_7.

A simple non-optimized FORTRAN code was written without any parallelization in computation. The computational time to reach a steady-state solution depended on the input physical parameters and the small nonzero damping rates α_{2m} which were employed to avoid beating in the symmetric modes. Normally, the damping rates $\alpha_{2m-1}=0$, $\alpha_{2m}=\xi_{2m}/10$ caused the computational time to be from 0.5 to 50 s to achieve a numerical steady-state solution within five significant figures (Intel(R) Core(TM) 2 Quad CPU (2.66 GHz) computer).

Our analysis starts with the experimentally lowest solidity ratio $Sn=0.4725$ leading to $K=3.09862$ according to formula (18). Comparing this value of K and $0.01^{-1/3}=4.6416$, one can conclude that condition (26) is satisfied *only* in an asymptotic sense. The adaptive modal method "feels" this fact. For the forcing frequencies close to $\sigma/\sigma_1^*=1$ simulations by the corresponding asymptotic modal systems were not able to get a clear steady-state solution with $\alpha_{2m-1}=0$ and $\alpha_{2m}<\xi_{2m}$. Physically, this means that other (in addition to the screen-induced one) damping mechanisms, including the viscous boundary layer at the wetted tank surface, matter for the present physical and geometric input parameters. The numerical results on the maximum steady-state wave elevation (1 cm at the wall) noted in Fig. 4 by solid lines were therefore obtained with $\alpha_{2m-1}=0$ and $\alpha_{2m}=\xi_{2m}$. These results are in a good agreement with experiments. For comparison, we present also the quasi-linear prediction from Ref. 1 by the dashed line.

For the case in Fig. 4, the adaptive modal method requires the four asymptotic modal systems M1, M2, M3, and M4 (see the ranges of their applicability on the figure top) to capture different *a posteriori* asymptotic relationships appearing on the whole interval $0.7<\sigma/\sigma_1^*<1.36$. These systems involve the following dominant modes: M1 = {1, 3, 5, 2}, M 2= {1, 5, 7, 9}, M3 = {1, 9, 11, 4}, and M4 = {1, 5, 7, 9, 11, 13, 15, 4, 6}. A requirement for being dominant is clarified by the secondary resonance as $i_3=0.625$, $i_2=0.762$, $i_5=0.808$, $i_7=0.956$, $i_9=1.084$, $i_4=1.085$, $i_{11}=1.198$, $i_{13}=1.303$, $i_6=1.328$, $i_{15}=1.400$, $i_{17}=1.491$. The dominant character of the corresponding modes was also checked by direct numerical simulations.

Appearance of the secondary resonances is clearly seen on the response curves at i_2, i_3, i_7, i_4, i_9, and i_6. Our primary attention is on the secondary resonance at i_7 where a hysteresis occurs with two non-connected branches (it is seen in the zoomed view) and to the combined i_9-and-i_4 resonance (the latter two resonances due to the second and third harmonics are situated very close to each other). The combined i_9-and-i_4 resonance leads to the two non-connected branches, b1 (lower) and b2 (upper). The branch b2 causes a narrow peak which is not experimentally supported for this solidity ratio while it is for higher solidity ratios, e.g., in Figs. 6 and 8, where appearance of the peak agrees with experimental measurements. Even though the experiments were performed by decreasing the forcing frequency after a steady-state sloshing with previous forcing frequency was reached, transients, most likely, caused the experimental values belonging to the lower branch to end at C1. There are no serious free-surface phenomena like (i–iii) (see, Introduction) in experimental observation at the frequency range close to C1, thus, the discrepancy cannot be related to the fact that the multimodal method does not capture specific free-surface motions. This cannot also be explained by accounting for the linear boundary layer damping for the antisymmetric modes. Indeed, including the non-zero linear damping terms ($\alpha_{2m-1}=\xi_{2m-1}$) in modal equations (23a) improves agreement with experiments for the forcing frequencies close to the primary resonance $\sigma/\sigma_1^*=1$, but these damping terms do not effect appearance of the theoretical peak.

Another interesting point is in the frequency range C2 (the i_7-zone with amplification of the third harmonics) where we have a quantitative discrepancy with experiments. The discrepancy can partly be explained by the local breaking waves which are found in experimental observations. Fig. 5 demonstrates a plunging wave breaker appearing near to the vertical walls for $\sigma/\sigma_1^*=0.9574$ belonging to C2.

Figs. 6–11 deal with the pressure drop coefficients K and $\bar{\eta}_{2a}$ for which condition (26) is satisfied. This means that the screen-induced damping should play the leading role for the antisymmetric modes. The linear damping terms play then a secondary role and are only needed in computations to reach the steady-state conditions. Later, they can pass to zero. Theoretical modeling of the experimental cases in Figs. 6–11 is therefore performed with $\alpha_{2m-1}=0$ and a decrease of α_{2m} from ξ_{2m} to $\alpha_{2m}<\xi_{2m}/10$ to get a numerical steady-state solution which is not affected by linear damping terms (as described in Sec. III C). Typically, the steady-state solution obtained with $\alpha_{2m-1}=0$ and $\alpha_{2m}=\xi_{2m}/10$ does not change (the difference is less than 0.1%) with subsequent decrease of α_{2m}. Furthermore, the same asymptotic modal systems M1, M2, M3, and M4 are used in these figures. These systems employ the modified Moiseev asymptotic ordering (25) revised due to the secondary resonance by the dominant ordering $O(\epsilon^{1/3})$ for the following modes: M1 = {1, 3, 5, 2, 4}, M2 = {1, 5, 7, 9, 2, 4}, M3 = {1, 5, 7, 9, 11, 13, 4}, and M4 = {1, 5, 7, 9, 11, 13, 15, 4, 6}. The frequency ranges for these models are shown in the figures.

The theoretical results for $Sn=0.6925(K=41.4063)$ are compared with experimental data in Fig. 6. For this screen,

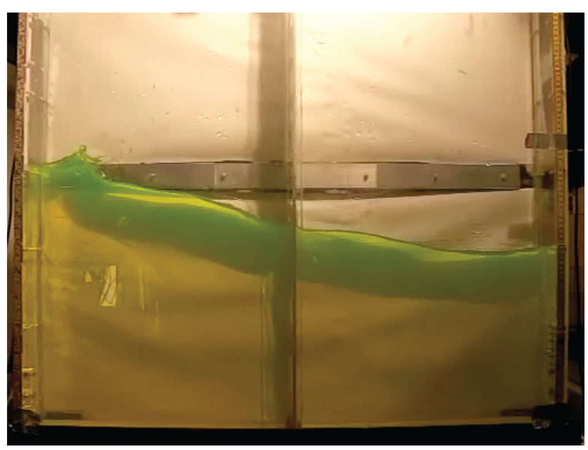

FIG. 5. (Color online) Video of the surface wave phenomena for the case in Fig. 4 with $Sn=0.4725$, $\eta_{2a}/l=0.01$ and $\sigma/\sigma_1^*=0.9574$. (enhanced online) [URL: http://dx.doi.org/10.1063/1.3602508.1]

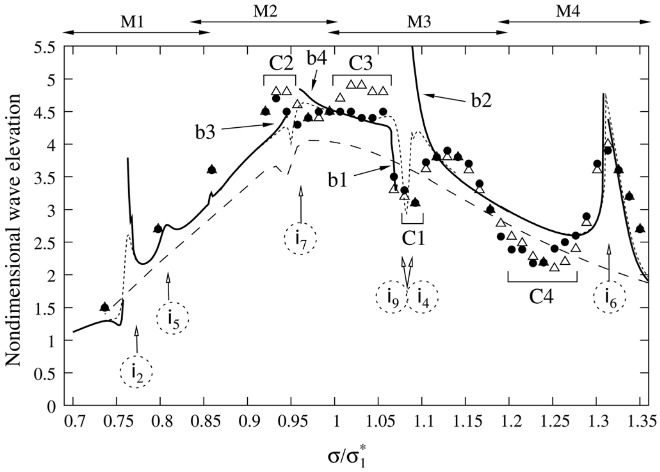

FIG. 6. The theoretical and experimental η_{2a}-scaled maximum wave elevation at the walls; $h/l = 0.4$, $\eta_{2a}/l = 0.01$. The signs (•) and (Δ) mark the experimental values. The submerged screen part has at rest 42 cross-openings (slots), $Sn = 0.6825$, and $K = 15.2292$ (due to (18)). The solid lines denote results by the adaptive multimodal method involving four asymptotic modal systems M1, M2, M3, and M4, whose frequency ranges are shown on the top. These adaptive modal systems employ the modified Moiseev asymptotic ordering (25) corrected due to the secondary resonance by the dominant ordering for the following modes: M1 = {1, 3, 5, 2, 4}, M2 = {1, 5, 7, 9, 2, 4}, M3 = {1, 5, 7, 9, 11, 13, 4}, and M4 = {1, 5, 7, 9, 11, 13, 15, 4, 6}. The asymptotic modal systems adopt $\alpha_{2m-1} = 0$ in Eq. (23a) but $\alpha_{2m} = \xi_{2m}/10$ in Eq. (23b) providing stabilization of the response curves as $\alpha_{2m} \to 0$. The dotted line shows the theoretical results with $\alpha_{2m} = \xi_{2m}$ in Eq. (23b). The dashed line (quasi-linear modal prediction) is taken from Faltinsen *et al.*[1] The values i_k are defined by Eqs. (1) and (2). They imply possibility of secondary resonance due to amplification of the second and third harmonics. The response curves are not connected between the branches b1 and b2 (a combined i_9-and-i_4 resonance), b3 and b4 (caused by the secondary resonance at i_7) as well as at i_6 and i_2.

the secondary resonances are expected at $i_3 = 0.624$, $i_2 = 0.762$, $i_5 = 0.807$, $i_7 = 0.955$, $i_9 = 1.084$, $i_4 = 1.085$, $i_{11} = 1.198$, $i_{13} = 1.303$, $i_6 = 1.328$, $i_{15} = 1.400$, and $i_{17} = 1.491$, i.e., they are almost the same as for the previous screen. Because we are able to test very small α_{2m}, our nonlinear modal theory shows four discontinuities (not two as in Fig. 4) in the response curves associated with the secondary resonances at i_2, i_7, i_9-and-i_4, and i_6. Agreement with experiments looks satisfactory. Experiments support the theoretical peaks at i_7,

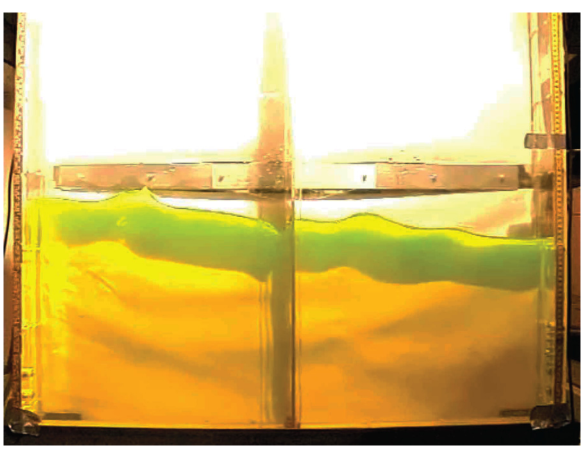

FIG. 7. (Color online) Video of the free-surface phenomena for the case in Fig. 6 with $Sn = 0.6825$, $\eta_{2a}/l = 0.01$ and $\sigma/\sigma_1^* = 1.043329$. (enhanced online). [URL:http://dx.doi.org/10.1063/1.3602508.2]

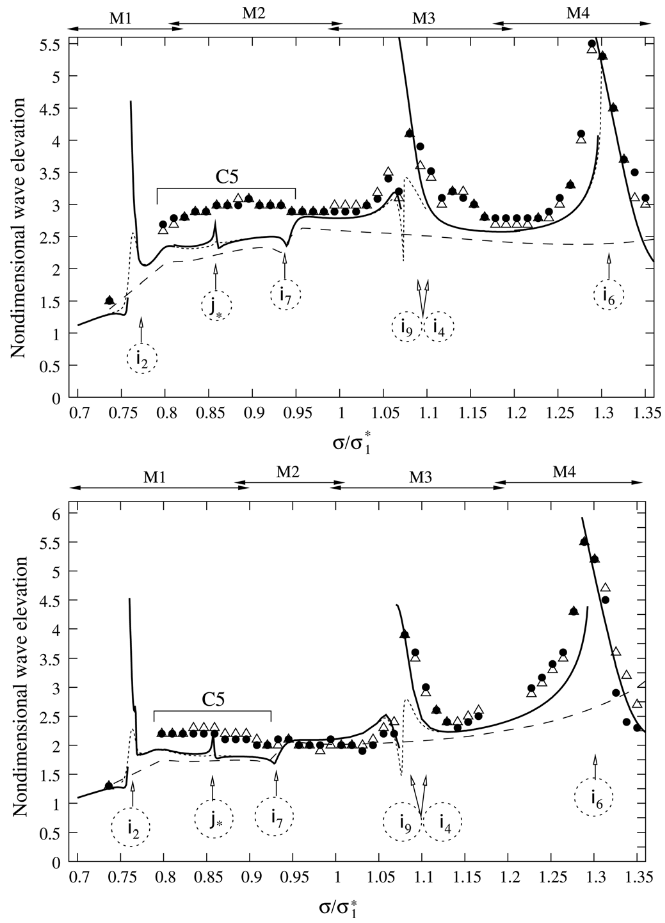

FIG. 8. The same as in Fig. 6 but for $Sn = 0.78625$, $K = 41.4063$, $N = 29$ (upper panel) and $Sn = 0.83875$, $K = 79.88.16$, $N = 22$ (lower panel). The frequency range C5 corresponds to the small-amplitude liquid sloshing where our nonlinear free-surface theory gives results close to the quasi-linear prediction, whereas both theoretical results on the maximum wave elevation at the walls are slightly lower than the experimental values.

i_9-and-i_4, and i_6. There are no appropriate experimental measurements at i_2. To demonstrate the damping effect on the symmetric modes due to the laminar boundary layer at the tank surface (the steady-state solution with $\alpha_{2m-1} = 0$, $\alpha_{2m} = \xi_{2m}$), we present the corresponding maximum theoretical wave elevations by the dotted line. This small damping does not modify the results from a qualitative point of view, but makes it possible to get fully connected response curves. Thus the mechanical system is *very sensitive* to the damping in a neighborhood of the secondary resonance points. Just around these points (see C1, C2, and C3) we see a quantitative discrepancy between our theory and experiments. As for a small frequency range C1 (see also, zone C1 in Fig. 4), the two experimental points in C1 do not belong to the theoretical branch b1 because this branch ends to the left of C1. Here, the linear damping due to the boundary layer at the wetted tank surface (dotted line, $\alpha_{2m-1} = 0$, $\alpha_{2m} = \xi_{2m}$) moves the branch end to the right. Thus, an improvement can be expected if we will be able to get a more accurate estimate of the global damping. The dotted lines show also a damping-related sensitivity in the zone C2. There is a discrepancy in the frequency range C3 where the measurements at the left and right measure probes differ from each other. In this

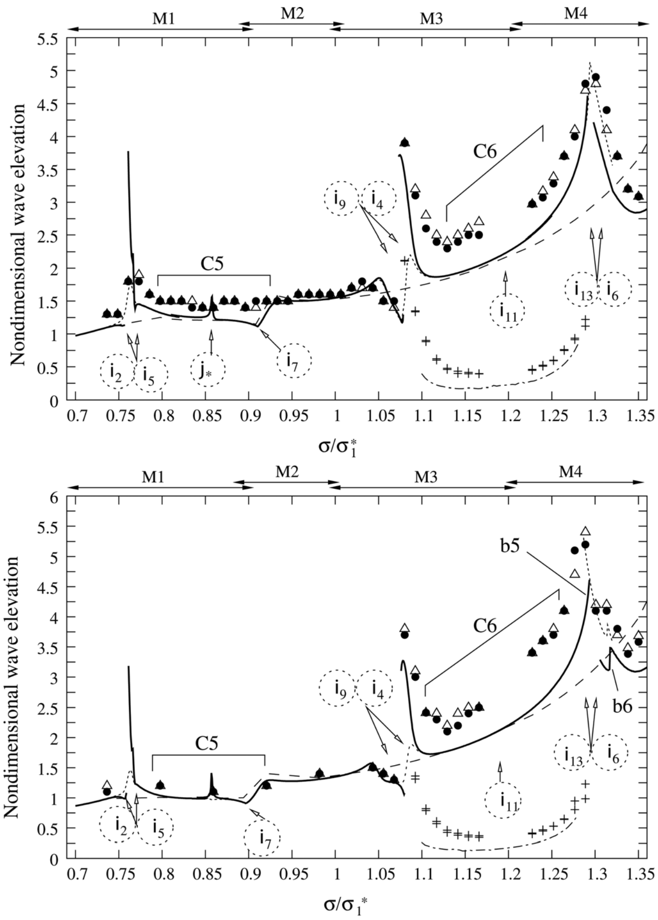

FIG. 9. The same as in Fig. 6 but for $Sn = 0.89125$, $K = 191.550$, $N = 15$ (upper panel) and $Sn = 0.91375$, $K = 315.503$, $N = 12$ (lower panel). The frequency range C5 corresponds to the small-amplitude sloshing where the nonlinear free-surface theory gives results on the steady-state wave elevations close to the quasi-linear prediction and both theoretical results are slightly lower than the experimental measurements. The frequency range C6 denotes a frequency range where a discrepancy occurs due to a larger double harmonics contribution to the measured signal (crests) relative to the theoretical prediction of this secondary harmonics (dashed-and-dotted line).

frequency range, the experiments show steep waves and a local breaking (see, video in Fig. 7). These phenomena may matter. A local wave breaking at the walls was also detected in the frequency range C4.

The theoretical results for $Sn = 0.78625$ and $Sn = 0.83875$ are compared with experimental measurements in the upper and lower panels of Fig. 8, respectively. For the screen with $Sn = 0.78625$, the most important secondary resonances are expected at $i_3 = 0.623$, $i_2 = 0.762$, $i_5 = 0.805$, $i_7 = 0.952$, $i_9 = 1.080$, $i_4 = 1.085$, $i_{11} = 1.194$, $i_{13} = 1.299$, $i_6 = 1.328$, $i_{15} = 1.400$, and $i_{17} = 1.491$. The screen with $Sn = 0.83875$ causes these secondary resonances at $i_3 = 0.621$, $i_2 = 0.762$, $i_5 = 0.803$, $i_7 = 0.950$, $i_9 = 1.078$, $i_4 = 1.085$, $i_{11} = 1.192$, $i_{13} = 1.296$, $i_6 = 1.328$, $i_{15} = 1.400$, and $i_{17} = 1.491$. For these two screens, we have, generally, a good agreement with experiments. A discrepancy appears in the frequency range C5, where the free-surface nonlinearity gives a minor contribution to the wave elevations except, very locally, at the point j_* so that the results by the adaptive modal method is the same as for the quasi-linear theory neglecting the free-surface nonlinearity. A narrow resonance at j_* is due to the fourth harmonics leading to the secondary resonance amplification of the tenth mode (theoretically, at $\sigma/\sigma_1^* = 0.8574252$). This amplification disappears when we include the linear damping terms with $\alpha_{2m-1} = 0$, $\alpha_{2m} = \xi_{2m}$ (dotted line). At the present time, we have no good explanation of the discrepancy at C5, but, because the results are almost the same as for the linear free-surface sloshing formulation in Ref. 1, this discrepancy cannot be explained by the free-surface nonlinearity. One interesting fact is a "knee" in the response curves at i_7 which is present for both linear and nonlinear free-surface theories. The "knee"-behavior is associated with the third harmonics yielded by the $(u|u|)$-nonlinearity in the pressure drop condition ($\bar{D}_m$-quantities in Eq. (23)) and, as we see, it is not influenced by the free-surface nonlinearity. The literature on the pressure drop condition does not give an answer on how precise this condition captures higher harmonics in the hydrodynamic pressure yielded by the viscous flow separation for the sinusoidal approach velocity. Normally, the literature discusses only the first harmonics and deals with the associated equivalent linearization. Furthermore, the terms $K\bar{D}_m$ come from Ref. 1 assuming an average over the mean wetted screen. This assumption may not be correct for higher solidity ratios causing a cross-flow through ΔSc (see Fig. 3).

Considering the experimental screens with higher solidity ratios leads to the results in Fig. 9. In the upper panel with $Sn = 0.89125$, $i_3 = 0.617$, $i_2 = 0.762$, $i_5 = 0.798$, $i_7 = 0.945$, $i_9 = 1.073$, $i_4 = 1.085$, $i_{11} = 1.187$, $i_{13} = 1.291$, $i_6 = 1.328$, $i_{15} = 1.399$, and $i_{17} = 1.491$, and the lower panel with $Sn = 0.91375$ implies $i_3 = 0.613$, $i_2 = 0.762$, $i_5 = 0.792$, $i_7 = 0.938$, $i_9 = 1.063$, $i_4 = 1.085$, $i_{11} = 1.176$, $i_{13} = 1.278$, $i_6 = 1.328$, $i_{15} = 1.398$, and $i_{17} = 1.490$. One can see that, because of the free-surface nonlinearity effect, the secondary resonance peak at i_6 moves to the left of its lowest-order prediction $i_6 = 1.328$ into the zone of the secondary resonance at i_{13}. This leads to a more complicated branch b6 (see also Fig. 11 to understand the tendency with increasing Sn) affected by a complex nonlinear interaction of the 6th and 13th modes. Including additional nonzero linear damping terms (here, $\alpha_{2m-1} = 0$, $\alpha_{2m} = \xi_{2m}$) gives a better agreement

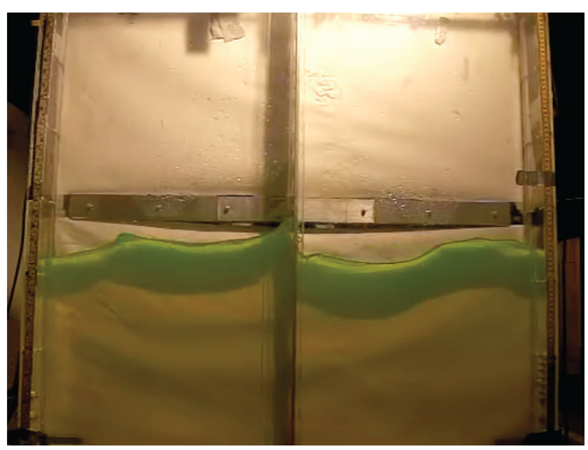

FIG. 10. (Color online) Video for the case in Fig. 9 (upper panel) with $Sn = 0.89125$, $\sigma/\sigma_1^* = 0.1288$. (enhanced online). [URL: http://dx.doi.org/10.1063/1.3602508.3]

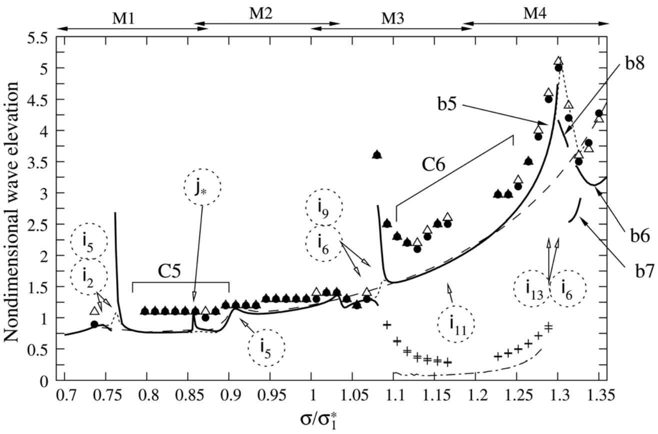

FIG. 11. The same as in Fig. 6 but for $Sn = 0.93625$, $K = 597.759$, and $N = 9$.

with experiments for the branch b6, but not for the branch b5. Fig. 10 shows the video for the steady-state sloshing associated with the top experimental point on the branch b5 in the upper panel of Fig. 9. The video demonstrates steep waves with local breaking and a pronounced jump in the free-surface profile at the screen. It is also clearly seen a flow from water to air through the screen area ΔSc. All these local free-surface phenomena may, generally, cause an extra dissipation which is not captured by the damping terms (22) with constant values of α_m.

The flow through ΔSc was also observed for the model tests conducted for the frequency range C6 (unfortunately, we do not have appropriate video). In this frequency range, the experimental signal (crests) contains a clearly larger second Fourier harmonics contribution relative to that by our nonlinear sloshing theory (dashed-and-dotted line). Our theory fully accounts for the quadratic free-surface nonlinearity which, from a mathematical point of view, is responsible for the second Fourier harmonics. Thus, we should look for other physical mechanisms generating this harmonics. For example, a dedicated analysis of the free-surface jump at the screen and related flow through ΔSc can, possibly, lead to the desirable second harmonics. We neglect the latter flow. In our pressure drop condition (19), the integration is not over the actual wetted screen (not from $-h$ to $\zeta_1(t)$ in Fig. 3) but over the mean wetted screen, i.e. from $-h$ to 0, which implies the lowest-order quantity in terms of small ζ_1 and ζ_2. If we speculatively integrate from $-h$ to ζ_1 in Eq. (19) and expand the obtained integral in a Taylor series by assuming $\zeta_1(t) = O\left(\epsilon^{1/3}\right)$, one gets

$$-K\frac{\alpha_m \kappa_{2m-1}}{4h\Lambda^{(0)}_{(2m-1)(2m-1)}}\left(\int_{-h}^{0}\left(\sum_{i=1}^{\infty}\frac{\dot{\beta}_{2i-1}}{\kappa_{2i-1}}U_i(z)\right)\times\left|\sum_{i=1}^{\infty}\frac{\dot{\beta}_{2i-1}}{\kappa_{2i-1}}U_i(z)\right|\mathrm{d}z-\underline{-\left(\sum_{i=1}^{\infty}\frac{\dot{\beta}_{2i-1}}{\kappa_{2i-1}}U_i(0)\right)\left|\sum_{i=1}^{\infty}\frac{\dot{\beta}_{2i-1}}{\kappa_{2i-1}}U_i(0)\right|f_1(0-)\beta_1}+\cdots\right). \quad (27)$$

Because $\beta_1 = O\left(\epsilon^{1/3}\right)$ and β_1 contains the nonzero first Fourier harmonics, the underlined quantity in Eq. (27) yields the second harmonics to appear in the modal equations for the antisymmetric modes. A dedicated theoretical analysis of whether the screen-induced free-surface jump causes a second Fourier harmonics effect is therefore needed.

The same underprediction of the second harmonics in the frequency range C6 is seen for the larger solidity ratio 0.93625 in Fig. 11. Again, it cannot be related to the free-surface nonlinearity. Here, $i_3 = 0.604$, $i_2 = 0.762$, $i_5 = 0.779$, $i_7 = 0.921$, $i_9 = 1.063$, $i_4 = 1.085$, $i_{11} = 1.158$, $i_{13} = 1.262$, $i_6 = 1.328$, $i_{15} = 1.383$, and $i_{17} = 1.487$. The most interesting in the figure is the appearance of a non-connected branching at the i_6-and-i_{13} secondary resonance. Here, we see the non-connected branches b5, b6, b7, and b8, which, however, become connected and sufficiently modified when we include the linear damping terms for the symmetric modes ($\alpha_{2m-1} = 0$, $\alpha_{2m} = \xi_{2m}$).

IV. CONCLUSIONS

A theoretical approach was developed to describe secondary resonance in a rectangular tank with a central slotted screen of high solidity ratio. The secondary resonance is well known for two-dimensional steady-state resonant liquid sloshing in a clean tank when the forcing frequency σ is close to the lowest natural sloshing frequency (see Chap. 8 in Ref. 9). For the finite liquid depth, the secondary resonance leads to amplification of the second and third natural sloshing modes caused by quadratic and cubic free-surface nonlinearities, and the corresponding second and third harmonics (2σ and 3σ), respectively. Because of the trigonometric algebra for the natural sloshing modes, non-commensurate spectrum and damping, one can find only two forcing frequencies where the secondary resonance phenomenon occurs. These frequencies are situated away from the primary resonance frequency and, therefore, can matter only by increasing the forcing amplitude. Inserting a central slotted screen with a high solidity ratio, $0.5 \lesssim Sn < 1$, modifies the natural sloshing modes and, as a consequence, the secondary resonance phenomenon qualitatively changes. Because of the screen, the secondary resonance amplification can, depending on the input geometric and physical parameters, happen at a certain number of frequencies close to the primary resonance and, thereby, the resonance response curves would have a multi-peak shape. Higher natural sloshing modes (not only second and third) can now be excited. The present paper gives a qualitative and quantitative prediction of these facts.

Our theoretical approach is based on the nonlinear adaptive multimodal method which was first proposed by Faltinsen and Timokha[4] as a generalization of the Moiseev-type asymptotic approach for clean tanks. The adaptive modal method is an efficient numerical-and-analytical approach for parametric studies of the steady-state resonant sloshing and gives a rather accurate prediction and explanation of the multi-branching and multi-peaks of the response curves. The method requires derivation of a polynomial-type nonlinear modal system which is a base for asymptotic modal systems accounting for dominant contribution of higher modes to the resonant liquid sloshing for certain frequency domains. Such a polynomial-type modal system was derived for two-dimensional and three-dimensional sloshing in rectangular tanks. The present paper revises the adaptive modal method for screen-equipped two-dimensional tanks. The revisions require changes in the Moiseev-type asymptotic ordering and a new prediction of the forcing frequencies at which the secondary resonance occurs. According to these revisions, a relatively large number of dominant modes should be included into the asymptotic analysis of steady-state resonance sloshing. The method assumes an incompressible liquid with irrotational flow except in a local neighborhood of the screen. Following Faltinsen *et al.*,[1] the viscous screen effect for the antisymmetric modes (which determines the cross-flow) is expressed by an "integral"-type pressure drop condition which leads to the corresponding integral quantities in the modal equations responsible for antisymmetric modes. This situation can, of course, change when using the proposed multimodal method and the pressure drop condition for a non-central location of the screen, or for several screens installed in the tank. Following Ref. 2 and the presented adaptive multimodal technique, one should then derive a revised nonlinear adaptive modal system where, depending on the number of screens and their position, the $(\cdot|\cdot|)$-integral quantities can appear in all the modal equations.

For the central screen case, the symmetric modes are theoretically not damped. This requires artificial linear damping terms in the modal equations responsible for the symmetric modes which help to reach steady-state solutions in our calculations. For the model tests case, decreasing the artificial damping rates α_{2m} leads to convergence of the numerical procedure with $\alpha_{2m} \lesssim \xi_{2m}/10$ (ξ_{2m} are the damping rates for *linear sloshing* due to the laminar viscous boundary layer at the mean wetted tank surface for the clean tank) so that, as for the clean tank case by Faltinsen and Timokha,[4] the secondary resonance jumps on the response curves are clearly detected with the damping rates lower then ξ_i. This means that laminar viscous layer plays a minor role in damping the symmetric modes in the studied case.

Even though the theoretical approach gives very good qualitative and, generally, good quantitative prediction of the experimental steady-state elevations, there is a discrepancy between theory and experiments in certain frequency ranges. This can partly be explained by the free-surface phenomena discussed in Ref. 1. Another possible reason for quantitative discrepancies is that the "integral"-type pressure drop condition cannot capture effects of specific flows at the screen with increasing solidity ratio when a free-surface jump between left and right screen sides occurs. Unfortunately, we were not able to measure this screen-caused jump ΔSc due to due to local phenomena at the screen region accompanied with the free-surface segmentation and jet flow through the holes. Our adaptive multimodal theory detects the maximum jump ΔSc at the primary resonance zone as well as at the secondary resonances by antisymmetric modes, i.e., when $\sigma/\sigma_1^* \approx i_{2k+1}$, $k \geq 1$. This is because of the central position of the screen which implies continuous symmetric modes. A dedicated study of these nearly screen flows is required. Furthermore, we need to express the damping due to tangential drag at the screen.

[1] O. Faltinsen, R. Firoozkoohi, and A. Timokha, Phys. Fluids **23**, 042101 (2011).
[2] O. M. Faltinsen and A. N. Timokha, J. Sound Vib. **330**, 1490 (2011).
[3] R. D. Blevins, *Applied Fluid Dynamics* (Krieger Publishing Company, Malabar, FL, 1992).
[4] O. M. Faltinsen and A. N. Timokha, J. Fluid Mech. **432**, 167 (2001).
[5] M. Hermann and A. Timokha, Math. Models Meth. Appl. Sci. **18**, 1845 (2008).
[6] J. R. Ockendon, H. Ockendon, and D. D. Waterhouse, J. Fluid Mech. **315**, 317 (1996).
[7] G. Wu, Ocean Eng. **34**, 2345 (2007).
[8] C.-H.Wu and B.-F. Chen, Ocean Eng. **36**, 500 (2009).
[9] O. M. Faltinsen and A. N. Timokha, *Sloshing* (Cambridge University Press, Cambridge, 2009).
[10] O. M. Faltinsen and A. N. Timokha, J. Fluid Mech. **470**, 319 (2002).
[11] M. Maravani and M. S. Hamed, Int. J. Numer. Methods Fluids **65**, 834 (2011).
[12] N. N. Moiseev, J. Appl. Math. Mech. **22**, 860 (1958).
[13] O. M. Faltinsen, J. Ship Res. **18**, 224 (1974).
[14] O. Faltinsen, O. Rognebakke, I. Lukovsky, and A. Timokha, J. Fluid Mech. **407**, 201 (2000).
[15] J. Love and M. Tait, J. Fluids Struct. **26**, 1058 (2010).
[16] J. Love, M. Tait, and H.Toopchi-Nezhad, Eng. Struct. **33**, 738 (2011).
[17] I. Lukovsky and A. Timokha, *Variational Methods in Nonlinear Problems of the Dynamics of a Limited Liquid Volume* (Institute of Mathematics of the National Academy of Sciences of Ukraine, Kiev, 1995) in Russian.
[18] R. E. Moore and L. M. Perko, J. Fluid Mech. **22**, 305 (1964).
[19] L. Perko, J. Fluid Mech. **35** (1), 77 (1969).
[20] M. La Rocca, M. Scortino, and M. Boniforti, Fluid Dyn. Res. **27**, 225 (2000).
[21] M. Tait, A. El Damatty, N. Isyumov, and M. Siddique, J. Fluids Struct. **20**, 1007 (2005).
[22] O. Faltinsen, O. Rognebakke, and A. Timokha, Phys. Fluids **18**, 012103 (2006).